

Interactions and Dynamics of Topological Defects: Theory and Experiments near the Onset of Weak Turbulence

Gilad Goren, Itamar Procaccia, Steffen Rasenat, and Victor Steinberg

Departments of Chemical Physics and Nuclear Physics, The Weizmann Institute of Science, Rehovot 76100, Israel

(Received 20 April 1989)

The dynamics of a single topological defect and the interaction between pairs, including the process of annihilation of defects of opposite topological charge, are studied experimentally and theoretically near the onset of weak turbulence in Williams domains of electroconvecting nematics. The existence of topological defects requires a gauge-field theoretical treatment, enriching the commonly used "amplitude equations." The gauge field carries the interaction which is found to be of finite range in agreement with detailed observations.

PACS numbers: 47.25.-c

Low-dimensional chaos appears in physical systems that are sufficiently constrained¹ to maintain spatial coherence in spite of the loss of temporal order. Small-aspect-ratio convecting systems, and efficiently stirred chemical reactors, are examples. In less constrained cases like large-aspect-ratio convecting systems, spatial coherence is lost concurrently with the onset of chaos, typically by the appearance of defects, whose complex dynamics carries much of the interesting time dependence. This regime of motion has been termed "spatio-temporal chaos," "weak turbulence," etc.²

The understanding of this type of turbulence calls for the elucidation of the interactions and motion of topological defects. In this Letter we report a joint experimental and theoretical attempt to reach such a goal near the onset of weak turbulence in electrodynamic convection in liquid crystals.³

The choice of a thin layer of nematic for this study is motivated by both experimental and theoretical considerations. Experimentally a treatment of the top and bottom boundaries allows the achievement of a perfectly ordered Williams domain even in samples of very large aspect ratio. This experiment employed N-(*p*-methoxybenzylidene)-*p*-butylaniline (MBBA) confined between transparent electrodes of dimensions $3 \times 0.7 \text{ cm}^2$. The thickness of the layer was $15 \mu\text{m}$, leading to about 2000 convection rolls. The fact that the molecules are anchored at the treated boundaries leads to a selection of a unique orientation of the convection rolls. Compared to isotropic fluids this leads to a simpler dynamical description ("amplitude equations") in the absence of topological defects.³ The needed modifications in the presence of defects are thus based on a simpler starting point.

Convection in this fluid is driven by an ac field of frequency ω across the layer. The control parameters are ω and ϵ , where $\epsilon = (V^2 - V_c^2)/V_c^2$ with V the amplitude of the potential and V_c its threshold value for the onset of convection. All measurements were taken at a fixed value of ω , i.e., $\omega^* = 114 \text{ Hz}$. The periodicity of the con-

vection pattern depends on the driving frequency, and this was used in the experimental procedure employed to investigate the dynamics of the defects: For a given frequency ω , ϵ is raised to a value such that many defect pairs are formed in the system. After relaxation to a state with only a few defects, and a wave vector $q(\omega)$ consistent with the frequency ω , the system was rapidly quenched back to $\omega = \omega^*$ and a chosen value of ϵ , consistent with an equilibrium wave vector $q(\omega^*)$, thus creating a wave-vector mismatch $k = q(\omega) - q(\omega^*)$. The motion of the defects on their way to pairwise annihilation was followed. For quantitative measurements,

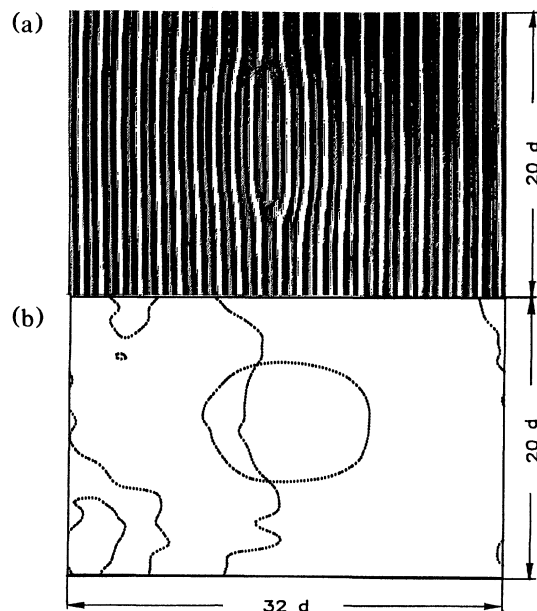


FIG. 1. (a) A shadowgraph (Ref. 11) of a Williams domain in a nematic with two defects of opposite topological charges. (b) A plot of the lines $\text{Im} A = 0$ (closed loop) and $\text{Re} A = 0$ (open curves) for the picture in (a). The points of crossing are the defect cores.

the exact location of the defects is needed. In standard shadowgraphs the image is formed by the field of index of refraction $n(\mathbf{x}, t)$, which can be represented as $n(\mathbf{x}, t) = A(\mathbf{x}, t)\exp(i\mathbf{q}\cdot\mathbf{x})$ where A is a complex amplitude, which vanishes at the defect core. We digitize the shadowgraph, perform a fast-Fourier transform (FFT), shift the spectrum such that its major peak moves to $q=0$, and transform back to real space. Plotting then the two curves $\text{Re}A=0$ and $\text{Im}A=0$, every intersection of these pinpoints a defect core. In Fig. 1 we show two topological defects using a standard shadowgraph and the technique discussed here. This technique allows pinpointing the core with a resolution of the order of $\pm 1 \mu\text{m}$.

In Figs. 2(a)–2(c) we show three typical plots of distance versus time of pairs of defects on their way to annihilation, measured this way, for three values of ϵ . The essential features to be noticed are as follows: (i) There exists a regime of constant relative velocity v_c of the defects; (ii) there exists a crossover distance R^* below which the motion accelerates; and (iii) the crossover distance R^* depends on v_c . In Fig. 3 it is shown that R^* is linear in $1/v_c$.

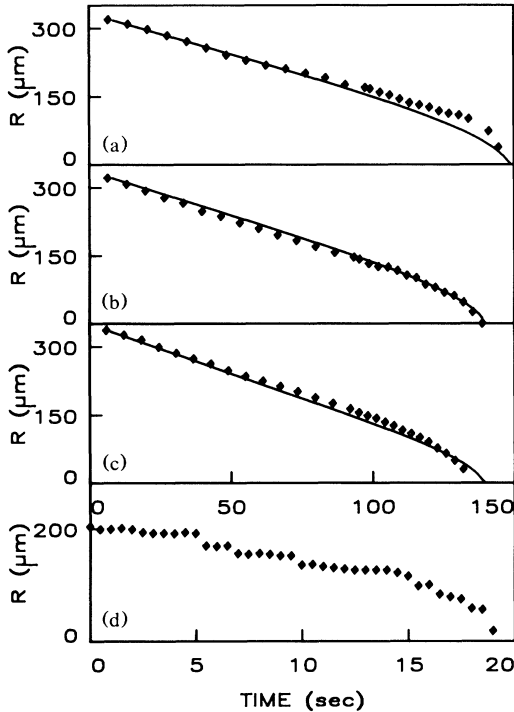


FIG. 2. Distances between two topological defects on their way to annihilation as a function of time. (a)–(c) The motion is both parallel and perpendicular to the roll axis (“climb” and “glide”), but predominantly climb. The continuous line is not a fit but the result of the theoretical calculation. The data pertain to ϵ values of 0.021, 0.033, and 0.08, respectively, and \bar{k} values of 0.0056, 0.0064, and 0.0077 μm^{-1} , respectively. (d) The motion is predominantly glide; notice the pinning effect that is due to the underlying roll structure.

We stress that the motion includes both “climb” and “glide;” Fig. 2(d) displays predominantly glide motion in which pinning effects which are tied to nonadiabatic effects⁴ are apparent.

In trying to understand these results we were motivated to develop a novel approach, as outlined next.

In the absence of defects one writes^{5,6} for any physical quantity $\psi(\mathbf{r}, t)$ that vanishes at $\epsilon=0$,

$$\psi(\mathbf{r}, t) = \text{Re}[\epsilon^{1/2}\chi(X, Y, T)\exp(i\mathbf{q}_{\text{eq}}\cdot\mathbf{x})f_{\psi}(z, t)],$$

where \mathbf{q}_{eq} is a 2D wave vector that sets the scale of the cellular convection, f_{ψ} lumps all the perpendicular direction and fast time dependences, and the amplitude χ is declared to be the only slowly varying (complex) field in the system, depending on the scaled space and time coordinates $X = \epsilon^{1/2}x$, $Y = \epsilon^{1/2}y$, and $T = \epsilon t$. The equation of motion for χ is well known and for normal rolls takes on the form

$$T_0 \partial_T \chi = [\xi_1^2 \partial_X^2 + \xi_2^2 \partial_Y^2 + 1 - \beta |\chi|^2] \chi + O(\epsilon^2).$$

The parameters can be computed from the underlying nematodynamics.³ Rescaling according to $t = T/T_0$, $x = X/\xi_1$, $y = Y/\xi_2$, and $\chi' = \sqrt{\beta}\chi$, we get (dropping the prime)

$$\partial_t \chi = (\nabla^2 + 1 - |\chi|^2) \chi, \quad (1)$$

which is the well-known time-dependent Ginzburg-Landau equation. This equation can be written in terms of a variational principle of the functional $I_f = \int d\mathbf{x} \tilde{I}_f(\mathbf{x})$, where

$$\tilde{I}_f(\mathbf{x}) = -|\chi|^2 + \frac{1}{2} |\chi|^4 + |\nabla \chi|^2. \quad (2)$$

Obviously, Eqs. (1) and (2) are invariant to the global

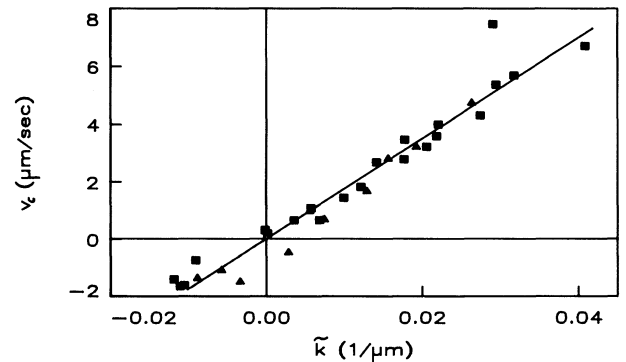


FIG. 3. The crossover distance R^* as a function of $1/v_c$. Inset: The interaction length λ as a function of $1/\sqrt{\epsilon}$. The length λ was obtained from the curves of distance vs time in an annihilation process. The values of R^* were obtained by fitting a straight line and a parabolic curve to the short- and long-time portions of the data of Fig. 2, respectively, and reading R^* from the discontinuity.

gauge transformation $\chi \equiv |\chi| e^{i\theta} \rightarrow |\chi| e^{i\theta+\phi}$. Indeed, topological defects can be understood in terms of the mapping from a large circle around the defect to different $\Theta(\mathbf{x})$ values in the space of degenerate vacuum solutions of Eq. (1). The defects seen in our experiment satisfy the relation $\oint \nabla\Theta \cdot d\mathbf{l} = \pm 2\pi$, where the opposite signs pertain to opposite topological charges. This relation indicates that Θ is undefined at the core, whereas $\nabla \times \nabla\Theta$ diverges there like $2\pi\delta(\mathbf{x})\hat{\mathbf{z}}$, where $\hat{\mathbf{z}}$ is the unit vector in the z direction. The main point, however, comes next, when we argue that in the presence of defects there may exist another conserved (slow) quantity which has to be coupled to the field χ . Consider the local \mathbf{k} vector $\mathbf{k}(\mathbf{x}) = \nabla\Theta(\mathbf{x})$ ($\mathbf{k} = \mathbf{q} - \mathbf{q}_{\text{eq}}$). In the absence of defects $\nabla \times \mathbf{k} = 0$. In the presence of defects $\nabla \times \mathbf{k} \neq 0$. In that case we rewrite $\mathbf{k}(\mathbf{x})$ as

$$\mathbf{k}(\mathbf{x}) = \nabla\Theta(\mathbf{x}) - \mathbf{A}(\mathbf{x}), \quad (3)$$

where \mathbf{A} is a gauge field. Here we have split \mathbf{k} into a part that has only a singular curl (i.e., $\nabla \times \nabla\Theta$) and a part that possesses a nonsingular curl, defined as

$$\mathbf{B}(\mathbf{x}) = \nabla \times \mathbf{A}. \quad (4)$$

Anywhere but at the center of the defect $\nabla \times \mathbf{k} = \nabla \times \mathbf{A}$. Using three-vector notation in this two-dimensional problem, $\mathbf{B} = (0, 0, B)$, $\mathbf{A} = (A_x, A_y, 0)$. By defining $\mathbf{E} = (E_x, E_y, 0)$ according to $\mathbf{E} = -\partial_t \mathbf{A}$, we get the topological conservation law

$$\partial_t \mathbf{B} = -\nabla \times \mathbf{E}. \quad (5)$$

\mathbf{B} is proportional to the density of defects, $\mathbf{E} \times \hat{\mathbf{z}}$ is its current, and Eq. (5) means that \mathbf{B} is an independent slow variable that has to be coupled to χ . Notice that Eq. (5) is independent of the nature of the amplitude equation (1), and is an independent construct of the theory. Also \mathbf{B} is not multiplied by $e^{i\mathbf{q} \cdot \mathbf{x}}$, meaning that it can be a large-scale field of the type considered in Refs. 5(b) and 7. The physics of these new fields has to do presumably with the interplay between the director of the nematic and flow velocities in the x - y plane. The latter cannot be assumed to be proportional to gradients of scalars as in Rayleigh-Bénard convection.

Before coupling, notice that \mathbf{B} is invariant to a local gauge transformation $\mathbf{A}(\mathbf{x}) \rightarrow \mathbf{A}(\mathbf{x}) + \nabla\alpha(\mathbf{x})$. In addition, the change of $\mathbf{k} = \nabla\Theta$ into Eq. (3) suggests that after coupling \mathbf{B} to χ all the derivatives should become covariant, i.e., $\nabla\chi \rightarrow \mathbf{D}\chi \equiv (\nabla - i\mathbf{A})\chi$.

The coupled functional $I_c \equiv \int d\mathbf{x} \tilde{I}_c(\mathbf{x})$ is defined therefore by $\tilde{I}_c = -|\chi|^2 + \frac{1}{2}|\chi|^4 + |\mathbf{D}\chi|^2 + \tilde{I}_d$, where \tilde{I}_d stands for the part proportional to \mathbf{B} . Symmetry and topology considerations lead to the following form for \tilde{I}_d :

$$\tilde{I}_d = \zeta(\frac{1}{2}B^2 - \mathbf{B} \cdot \mathbf{M}), \quad (6)$$

where ζ is a coupling constant and \mathbf{M} is a pseudovector field $\mathbf{M} = (0, 0, M)$, having the same signature under parity as \mathbf{B} . The only pseudovector at our disposal is $\mathbf{k} \times \mathbf{x}$,

and it will indeed follow from consistency requirements on the equations of motion that \mathbf{M} is proportional to $\mathbf{k} \times \mathbf{x}$.

The equations of motion are found now by varying I_c with respect to χ , χ^* , and \mathbf{A} . The result of this procedure is

$$\partial_t \chi = (\mathbf{D} \cdot \mathbf{D} + 1 - |\chi|^2)\chi, \quad (7a)$$

$$\sigma \partial_t \mathbf{A} = \mathbf{J} - \zeta \nabla \times \mathbf{H}, \quad (7b)$$

where $\mathbf{H} \equiv \mathbf{B} - \mathbf{M}$ and

$$\mathbf{J} = i\chi(\mathbf{D}\chi)^* + \text{c.c.} = 2|\chi|^2[\nabla\Theta - \mathbf{A}]. \quad (8)$$

σ is a typical time scale for the gauge field.

The detailed solution of this gauge-field theory is presented elsewhere.⁸ Here we only summarize the results, and tie them to the experiment.

(i) In the absence of topological defects we find that $|\chi|^2 = 1 - k^2$ and $\mathbf{B} = 0$. On the other hand, we find that $\mathbf{M}(\mathbf{x})$ satisfies the expected relation

$$\mathbf{M}(\mathbf{x}) = -(1/\lambda^2)(1 - |\chi|^2)^{1/2} \hat{\mathbf{k}} \times \mathbf{x}, \quad (9)$$

where $\hat{\mathbf{k}} = \mathbf{k}/k$ and λ is an important length scale in our theory,

$$\lambda = \left[\frac{\zeta}{2|\chi|^2} \right]^{1/2} = \left[\frac{\zeta}{2(1-k^2)} \right]^{1/2}. \quad (10)$$

We thus see that M vanishes only in the unstressed cellular state where $|\chi|^2 = 1$.

(ii) For a single stationary defect on an unstressed background ($\mathbf{k} = 0$) the field \mathbf{B} satisfies the London equation $\mathbf{B} + \lambda^2 \nabla \times \nabla \times \mathbf{B} = 2\pi \delta(\mathbf{x}) \hat{\mathbf{z}}$ or $\mathbf{B}(\mathbf{x}) = -(1/\lambda^2) K_0(x/\lambda) \hat{\mathbf{z}}$, where K_0 is the modified Bessel function of order zero. For such \mathbf{B} we find that

$$\mathbf{k} = \nabla\Theta - \mathbf{A} = (1/\lambda) K_1(x/\lambda) \hat{\theta} = (\lambda^2/\zeta) \mathbf{J}, \quad (11)$$

where $\hat{\theta}$ is a unit vector perpendicular to \mathbf{x} . We note that at this level the solution for \mathbf{B} is identical to that of a magnetic field of a magnetic flux line in a superconductor of type II without external magnetic field.⁹ \mathbf{J} is the analog of the supercurrent around it, and it goes to zero exponentially for distances much larger than λ . Also $\mathbf{A} \rightarrow \nabla\Theta$ far from the defect.

(iii) In a stressed background field we split the vector \mathbf{k} into a defect contribution $\tilde{\mathbf{k}}$ and a background part \mathbf{k} . For $\tilde{\mathbf{k}} \neq 0$ there is a force on a single defect, and it moves with a constant velocity v_c , which is determined by a mobility tensor. In the adiabatic approximation (i.e., $\sigma \ll 1$) we solve for the mobility tensor γ , and find a perfectly finite solution,

$$\gamma \approx 2\pi |\chi|^2 [\ln(\lambda/\xi) + \frac{1}{4} \pi e^{-2}] \mathbf{1}, \quad (12)$$

where ξ is the size of the defect core, and $\mathbf{1}$ is the unit tensor.

To calculate the velocity we need the force. The force \mathbf{F}_s acting on a defect due to a background is calculated

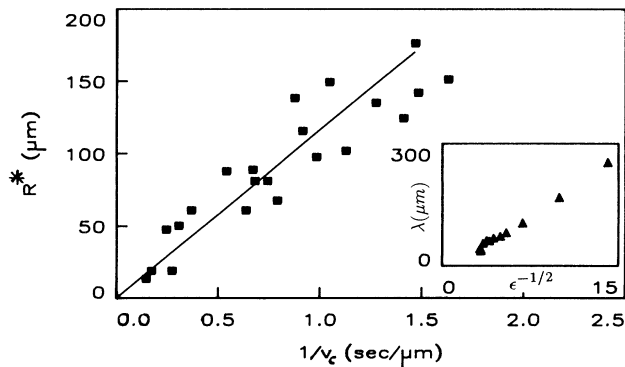


FIG. 4. The constant velocity of an isolated defect as a function of the wave-vector mismatch \tilde{k} . Squares: $\epsilon=0.06$. Triangles: $\epsilon=0.03$.

by finding the gradient of the functional I_c with respect to the position of the defect. The result is

$$\mathbf{F}_s \approx (2\pi\zeta/\lambda^2)\tilde{\mathbf{k}} \times \hat{\mathbf{z}} - (2\pi\zeta/\lambda^2)(\nabla\tilde{\Theta} - \tilde{\mathbf{A}}) \times \mathbf{z} - \tilde{\mathbf{J}} \times 2\pi\hat{\mathbf{z}}, \quad (13)$$

where $\tilde{\mathbf{J}}$ is the current (8) due to the background. The part of the force proportional to $\nabla\tilde{\Theta} \times \hat{\mathbf{z}}$ is known as the Peach-Koehler force. This by itself is not the correct force, as was pointed out first in Ref. 10.

The velocity of a single defect is obtained by equating $\tilde{\mathbf{F}}_s$ to $\gamma \cdot \mathbf{v}_c$. The magnitude of the constant velocity is predicted to be

$$v_c = 2\tilde{k}[\ln(\lambda/\xi) + \frac{1}{4}\pi\epsilon^{-2}]^{-1}. \quad (14)$$

(iv) Defects interact via a force directed along the interdefect separation vector \mathbf{R} . Leaving one defect at the origin of the coordinates we calculate the interaction force $\mathbf{F}_I(\mathbf{R})$ and find

$$\mathbf{F}_I(\mathbf{R}) = (2\pi\zeta/\lambda^3)K_1(R/\lambda)\hat{\mathbf{R}}. \quad (15)$$

This force depends on R like $1/R$ for $R < \lambda$ and like $(1/\sqrt{R})e^{-R/\lambda}$ for $R > \lambda$.

These theoretical findings are in very good agreement with the experimental facts reported before. First, we expect that for distances $R > \lambda$ the defects would hardly interact, and their constant velocity (cf. Fig. 2) should satisfy Eq. (14). To test this explicitly we display in Fig. 4 the experimental plot of v_c vs \tilde{k} . \tilde{k} is measured from the FFT of the digitized picture with the defects, and from $q_{\text{eq}}(\omega^*, \epsilon)$ that is measured in a separate experiment. The agreement with Eq. (14) is obvious. Moreover, from the slope of Fig. 4 we can extract the only parameter of the theory, i.e., ζ , which is found to be $\zeta=83$, which determines $\lambda \approx 6.5\xi$. Thus, the rest of the comparisons between the theory and the experiment will

have no free parameter.

We expect that the motion will begin to accelerate only when F_I becomes comparable to F_s . This happens at an R value which solves the equation $\tilde{k}/\lambda^2 \sim K_1(R^*/\lambda)/\lambda^3$. Using the form $K_1(R/\lambda) \sim \lambda/R$ for $R \lesssim \lambda$, we find $R^* \approx 1/\tilde{k}$. In the light of the linearity of v_c in \tilde{k} , we understand the finding displayed in Fig. 3. Finally, the detailed trajectories R vs t can be found by solving the equation $\gamma \cdot \dot{\mathbf{R}} = \mathbf{F}_s + \mathbf{F}_I(\mathbf{R})$. This equation is solved in scaled coordinates. To compare with the laboratory plots we have to rescale to real coordinates. The parameters used are $\tau_0=0.075$ sec, $\xi_1/\xi_2=2.2$, and $\xi_2=2.2$ μm , and were taken from separate experiments which will be reported in detail elsewhere. The results of this calculation, which at this point has no free parameter, are shown as the continuous lines in Fig. 2. The agreement should be interpreted as a strong confirmation of the theory sketched above. As a final test we examined the scaling of λ with ϵ . The inset in Fig. 3 shows that λ is linear in $1/\sqrt{\epsilon}$ as predicted.

This work has been supported in part by the Minerva Foundation, Munich, Germany, and the GIF (German-Israeli Foundation). Discussions with E. Bodenschatz, I. Rehberg, and L. Kramer are acknowledged.

¹P. Berge, Y. Pomeau, and C. Vidal, *Order within Chaos* (Wiley, New York, 1984).

²G. Ahlers and R. P. Behringer, *Phys. Rev. Lett.* **40**, 712 (1978); J. P. Gollub and J. K. Steinman, *Phys. Rev. Lett.* **47**, 505 (1981); G. Ahlers, D. S. Cannell, and V. Steinberg, *Phys. Rev. Lett.* **54**, 1373 (1985); A. Pocheau, V. Croquette, and O. LeGal, *Phys. Rev. Lett.* **55**, 1099 (1985); P. Couillet, L. Gil, and J. Lega, *Phys. Rev. Lett.* **62**, 1619 (1989).

³See, e.g., E. Bodenschatz, W. Zimmermann, and L. Kramer, *J. Phys. (France)* **49**, 1875 (1988), and references therein.

⁴Y. Pomeau, *Physica (Amsterdam)* **23D**, 3 (1986).

⁵(a) E. D. Siggia and A. Zippelius, *Phys. Rev. A* **24**, 1036 (1981); (b) A. Zippelius and B. Siggia, *Phys. Fluids* **26**, 2906 (1983); (c) Y. Pomeau, S. Zaleski, and P. Manneville, *Phys. Rev. A* **27**, 2710 (1983); (d) G. Tesauro and M. C. Cross, *Phys. Rev. A* **34**, 1363 (1986).

⁶E. Bodenschatz, W. Pesch, and L. Kramer, *Physica (Amsterdam)* **32D**, 135 (1988).

⁷A. Pocheau, in *Propagation in Systems Far from Equilibrium*, edited by J. Wesfreid, H. Brand, P. Manneville, G. Albiñet, and N. Boccara (Springer-Verlag, Berlin, 1988), p. 156.

⁸G. Goren and I. Procaccia (to be published).

⁹D. Saint-James, G. Sarma, and E. J. Thomas, *Type II Superconductivity* (Pergamon, Oxford, 1969).

¹⁰K. Kawasaki, *Prog. Theor. Phys. Suppl.* **79**, 161 (1984).

¹¹S. Rasenat, G. Hartung, B. L. Winkler, and I. Rehberg, *Exp. Fluids* **7**, 412 (1989).